Journal of Wind Engineering & Industrial Aerodynamics 178 (2018) 57–68

Contents lists available at ScienceDirect

Journal of Wind Engineering & Industrial Aerodynamics

journal homepage: www.elsevier.com/locate/jweia

Numerical simulation of rime ice on NREL Phase VI blade

Liangquan Hu, Xiaocheng Zhu *, Jinge Chen, Xin Shen, Zhaohui Du

School of Mechanical Engineering, Shanghai Jiaotong University, Shanghai, 200240, China

ARTICLE INFO

Keywords:
Wind turbine
Rime ice
NREL Phase VI blade
Blade icing

ABSTRACT

Wind turbine installation in cold regions is prone to icing events. In this study, rime ice on the rotating NREL Phase VI blade is simulated. First, an icing model is developed and validated to gain a better understanding of blade icing. For the fixed airfoil, the root-mean-square error of the collection efficiency is 8.6%. The ice shape area error is 1.5%. For the rotating blade, the ice shape area error is 2.4%. The validation results indicate that the accuracy of the icing model is satisfactory. Second, rime ice on the NREL Phase VI blade is examined. The results suggest that ice mainly accretes on the blade leading edge. The ice thickness gradually increases along the radial direction. The maximum ice thickness can reach 7.7 cm. Finally, ice mass and power degeneration distributions are investigated. The results indicate that ice mass increases along the radial direction. The increase in the ice mass is up to 105.3%. The power mainly degenerates at the outer blade. The decrease in the power is up to 13.3%. With respect to anti/de-icing, increased attention should be focused on the outer blade.

1. Introduction

Currently, there is a tremendous strain on the worldwide energy supply, environmental pollution, and global warming. Significant attention has been focused on forcing a transition from nonrenewable energy resources (e.g., nuclear energy, fuel coal, and fossil oil) to renewable energy resources (e.g., ocean, wind, and solar energies) (Bengt and Wu, 2015). Renewable energy resources currently account for approximately 10% of the global energy demand and are expected to grow to satisfy 60% of the global energy demand by 2050 (Bengt and Wu, 2015). Among the renewable energy resources, wind energy, which is mainly applied for electricity generation by using wind turbine is renewable and clean, and does not adversely affect the environment (Bengt and Wu, 2015). In order to ensure that the wind energy fully reaches its potential, wind farms with a rich wind resource must be effectively used. The power is proportional to the cube of the wind speed, and thus, the capacity of a site is highly dependent on the wind speed as well as other factors including the design, layout, and turbine size (Barber et al., 2011). Many favorable sites are located in cold regions with higher altitude. In these regions, the wind speed increases approximately by 0.1 m/s per 100 m of altitude within the first 1000 m, and the available wind energy is approximately 10% higher than those in other regions due to the higher air density (Parent and Ilinca, 2011). However, these regions are innately susceptible to atmospheric icing events during winter seasons (Hu et al., 2017a).

Icing is caused by the impingement of the super-cooled water droplets. Based on different icing conditions, ice shapes on the blade are categorized into the following three types: glaze ice, rime ice, and mixed ice (Han et al., 2012). Glaze ice is formed when a portion of the super-cooled water droplets do not immediately freeze after impingement. The water runs back and freezes later. It occurs at relatively warmer temperatures (above −10 °C), higher liquid water content, and higher median volumetric diameter. Glaze ice is rather transparent, hard, and firmly attaches to the surface (Fortin and Perron, 2009). Rime ice is formed when the super-cooled water droplets immediately freeze after impingement. It occurs at relatively colder temperatures (below −10 °C), lower liquid water content, and lower median volumetric diameter. Rime ice is white and opaque owing to air bubbles that are trapped inside the ice (Battisti, 2015). Mixed ice corresponds to a form between glaze ice and rime ice. It exhibits both the round leading edge rime ice shape and protruding ice feathers at the back of the ice shape that resembles glaze ice (Han et al., 2012).

Icing wind tunnel experiment and numerical simulation are two commonly used methods to perform a deep analysis of blade icing, (Blasco et al., 2017; Homola et al., 2012). The former method uses a refrigerator to create low temperature and sprays water droplets into the air to simulate real atmospheric icing conditions. The most famous icing wind tunnel is the NASA Icing Research Tunnel. It has been prevalently used for decades by the aircraft industry for safety certification, and is also introduced in the wind turbine industry for ice prediction and

* Corresponding author.
E-mail address: zhxc@sjtu.edu.cn (X. Zhu).

https://doi.org/10.1016/j.jweia.2018.05.007
Received 26 August 2017; Received in revised form 9 May 2018; Accepted 9 May 2018

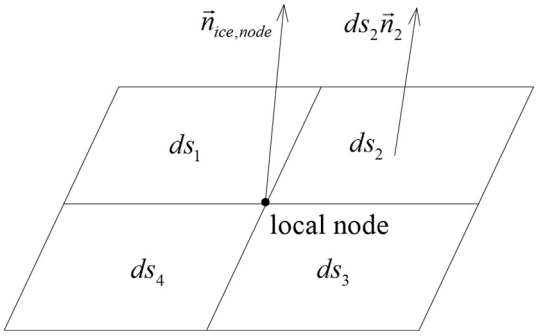

Fig. 1. Schematic diagram of the area-weighted average method..

Table 1
Icing conditions for the NACA0012 airfoil.

Chord length (m)	0.53
Free stream velocity (m/s)	105.4 and 58.1
Angle of attack (°)	4
Water droplets diameter (μm)	20
Liquid water content (g/m^3)	1.3
Ambient pressure (Pa)	95,610
Ambient temperature (K)	245.2
Icing time (min)	6

performance evaluation (Han et al., 2012). Icing wind tunnel experimental results are reliable. However, the operation and the maintenance costs are expensive, and thus, only a few research institutions can afford the same. The latter method, namely, numerical simulation, is less expensive and more convenient to apply. Therefore, it attracts significant attention. Numerical simulation of icing includes four basic steps (Hasanzadeh et al., 2013): 1. An aerodynamic solver calculates the air flow around the geometry. 2. Water droplet collection efficiency is calculated by the Lagrangian method or Eulerian method. 3. Thermodynamic analysis determines the ice amount. 4. A new surface is updated by a distance equivalent to the ice thickness. The above four steps have embedded in icing software, such as LEWICE and FENSAP-ICE.

In terms of wind turbines, the rotating blade can cause a significant radial flow. Meanwhile, the blade radial geometry is generally twisted and tapered. Fu et al. (Fu and Farzaneh, 2010) used the Eulerian multiphase flow model of ANSYS Fluent to simulate rime ice on the NREL VI turbine. It has three blades with a diameter of 11 m. In this study, an icing model to simulate rime ice on the rotating NREL Phase VI turbine is developed, and it is based on ANSYS Fluent user-defined functions (UDFs). This turbine has two blades with a diameter of 10.058 m. The remainder of this study is organized as follows: In Section 2, an icing model is described. In Section 3, ice shapes on the fixed and rotating geometries are validated. In Section 4, rime ice on the rotating NREL Phase VI blade is investigated. In Section 5, ice mass and power degeneration distributions are studied. The concluding remarks are discussed in Section 6.

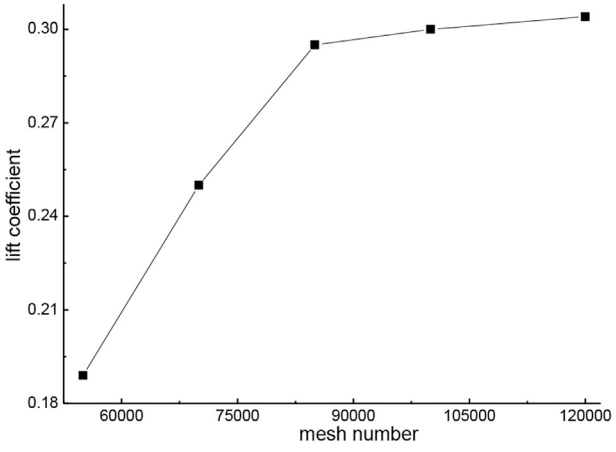

Fig. 2. Effect of the mesh refinement for the NACA0012 airfoil.

2. Icing model description

2.1. Calculation of air flow

In reality, icing is a transient phenomenon, and ice shape changes during accretion (Pedersen and Sørensen, 2016). In this study, icing is treated as a quasi-steady process. Therefore, the two-phase flow that is composed of the air and water phases is calculated by the steady solver.

In order to calculate the rotating air flow, the ANSYS Fluent moving reference frame (MRF) is used. A detailed description of the MRF is found in Ref. (ANSYS FLUENT Theory Manual; ANSYS FLUENT User's Guide). In ANSYS Fluent interface, the steady solver and k-ω SST turbulence model are selected. The SIMPLE method is used for the pressure-velocity coupling solution. The second order upwind is used for the discretization schemes. The convergence criteria for the residuals are specified as 10^{-6}.

2.2. Calculation of collection efficiency

After the air phase is calculated, the water droplet collection efficiency is calculated by using the Eulerian method. The Eulerian method treats the water droplets as a continuous phase, and uses the concept of volume fraction to represent the amount of water within a given control volume. Based on the concept, the conservation equations for the water phase are derived and solved just as the air phase (Tong and Luke, 2005). The water phase conservation equations in the Eulerian frame are expressed as equations (1) and (2) (Wirogo and Sirirambhatla, 2003). ANSYS Fluent provides an interface for researchers to define additional user-defined scalar (UDS) transport equations. Equations (1) and (2) are treated as scalar transport equations and added in ANSYS Fluent. A detailed description of the UDS transport equations is found in Ref. (ANSYS FLUENT UDF Manual).

$$\frac{\partial(\alpha\rho_d)}{\partial t} + \nabla\cdot(\alpha\rho_d \vec{u}_{da}) = 0 \tag{1}$$

$$\frac{\partial(\alpha\rho_d \vec{u}_{da})}{\partial t} + \nabla\cdot(\alpha\rho_d \vec{u}_{da}\vec{u}_{da}) = \alpha\rho_d \vec{g} + \alpha\rho_d K(\vec{u}_a - \vec{u}_{da}) \tag{2}$$

where α denotes the water droplet volume fraction, ρ_d denotes the water droplet density, $\vec{u}_{da}$ denotes the water droplet absolute velocity vector, $\vec{g}$ denotes the gravity acceleration vector, $\vec{u}_a$ denotes the air absolute velocity vector, and K denotes the exchange coefficient that is expressed in equation (3) as follows (Wirogo and Sirirambhatla, 2003):

$$K = \frac{18\mu_a f}{\rho_d d_d^2} \tag{3}$$

where μ_a denotes the air viscosity, d_d denotes the water droplet diameter, and f denotes the drag function that is expressed in equation (4) as follows (Wirogo and Sirirambhatla, 2003):

$$f = \frac{C_d R_e}{24} \tag{4}$$

where C_d denotes the drag coefficient, and R_e denotes the relative Reynolds number that is based on the relative velocity between the air phase and water phase. The formulae of the two parameters are expressed in equations (5) and (6) as follows (Bourgault et al., 1997):

$$C_d = \begin{cases} 24\left(1 + 0.15R_e^{0.687}\right)/R_e, & R_e \le 1000 \\ 0.44, & R_e > 1000 \end{cases} \tag{5}$$